Shape-selective organic-inorganic zeolitic catalysts prepared via interlayer expansion

Trees De Baerdemaeker [a], Wannes Vandebroeck [a], Hermann Gies [b], Bilge Yilmaz [c], Ulrich Müller [d], Mathias Feyen [d] and Dirk De Vos [a*]

[a] Centre for Surface Chemistry and Catalysis, KU Leuven, Kasteelpark Arenberg 23, 3001, Leuven, Belgium;

[b] Institute of Geology, Mineralogy and Geophysics, Ruhr-University Bochum, 44780, Bochum, Germany;

[c] BASF Corporation, Chemicals Research and Engineering, Iselin, NJ 08830, USA;

[d] BASF SE, Chemicals Research and Engineering, 67056, Ludwigshafen, Germany

Corresponding author
Dirk.DeVos@biw.kuleuven.be
Kasteelpark Arenberg 23, Post box 2461
3001 Heverlee
Belgium
Tel: (32)16321639

Abstract

Interlayer expansion of layered zeolite precursors is achieved via the insertion of an additional T-atom in between the layers, typically by means of a silylating agent as source of the T-atom. (3-mercaptopropyl)methyldimethoxysilane was used as Si-source in the interlayer expansion of the layered zeolite precursors RUB-36 and RUB-39. The structure expansion was confirmed with PXRD. The incorporation of the silylating agent was followed with ^{29}Si MAS NMR, ^{13}C CP MAS NMR and thermogravimetric analysis. The incorporated thiol groups were oxidized with H_2O_2 to obtain sulphonic acid groups in between the layers. ^{13}C CP MAS NMR was used to characterize the organic species and monitor the conversion of thiol to propylsulphonic groups. The shape-selective properties of the obtained materials were investigated in acid-catalyzed tetrahydropyranylation reactions.

Keywords

Interlayer expansion reaction, functionalized micropores, sulphonic acid, tetrahydropyranylation, shape selectivity, organic-inorganic hybrid

1 Introduction

Layered zeolite precursors are versatile building blocks for the synthesis of zeolitic catalysts. Besides their transformation into fully three-dimensionally connected zeolite frameworks by topotactic condensation of the silicate sheets, the layers can be rearranged in a variety of ways. Examples are interlayer expansion by placing an additional T-atom in between the layers, or swelling followed by pillaring, delamination or recombination of the sheets [1-8]. The resulting materials differ from their corresponding zeolite condensation products in pore size and shape, accessibility of active sites in the layers, sorption characteristics and other physicochemical and catalytic properties. In the case of interlayer expansion, typically a silylating agent containing two methyl- and two leaving groups (chloro-, ethoxy-) is used to link the opposite layers of the precursor instead of directly connecting those layers. This is illustrated in figure 1 for RUB-36, the layered zeolite precursor consisting of the ferrierite-type layer, which can be condensed to the three-dimensionally connected zeolite RUB-37 (CDO topology) or interlayer expanded with dichlorodimethylsilane (DCDMS) to the methyl group-containing, hydrophobic COE-3 [9]. As another example, the layered silicate RUB-39, which consists of heulandite-type layers, can be condensed to RUB-41 (RRO topology) or interlayer expanded to COE-1 [10, 11].

Figure 1. Materials derived from layered zeolite precursors RUB-36 (A) and RUB-39 (B). Displayed are the layered precursors (1) and the products of topotactic condensation (2) and interlayer expansion with DCDMS (3) or with 3-MPS (4) followed by oxidation with H_2O_2. Framework O-atoms and the organic SDAs in the layered precursors are omitted for clarity. In the case of RUB-39, two linking sites eclipsing each other are shown.

One way of introducing catalytic activity into the materials derived from layered, siliceous zeolite precursors is the isomorphous substitution of Al or other heteroatoms in the silicate layer [4, 5, 12-15]. Alternatively, the layers themselves can also serve as a support for catalytic sites through *e.g.* grafting of a metal precursor, or by creating hybrid organic-inorganic materials using organosilanes [16-18]. One interesting possibility is selectively placing the active sites in between the layers. Corma and co-workers used for instance 1,4-bis(triethoxysilyl)benzene as organic linking group between the layers of Al-containing MCM-22. Subsequent amination of the organic linkers introduced basic functionalities in close proximity of the layer-associated acid sites, resulting in a bifunctional catalyst [19].

In previous reports on the interlayer expansion of RUB-36 and RUB-39, the possibility of introducing reactive functional groups via interlayer expansion has been suggested [9, 11]. In this contribution, we demonstrate one of these possibilities by altering the interlayer expansion protocol to introduce sulphonic acid sites in between the layers, consequently obtaining a hybrid catalyst with acid sites placed selectively inside the interlayer gallery of the inorganic zeolite. Similar types of organic-inorganic hybrid catalysts containing propylsulphonic groups have been used in e.g. tetrahydropyranylations for the protection of alcohols, in bisphenol A synthesis, acetalizations, condensation of acetone and 2-methylfuran and esterifications [20-25]. We have modified the interlayer expansion by using a silylating agent containing besides two leaving groups also one methyl group and an alkylthiol group, which can be oxidized to a sulphonic acid group. The appropriate conditions for this oxidative transformation have been investigated. Finally, the acid and shape-selective properties of the functionalized catalysts in the protection of alcohols via tetrahydropyranylation were explored.

2 Experimental

2.1 Catalyst synthesis

2.1.1 Synthesis of the layered precursors:

Purely siliceous RUB-36 and RUB-39 were synthesized according to references [9] and [10] using the respective organic structure directing agents (SDA) diethyldimethyl ammonium hydroxide and dimethyldipropyl ammonium hydroxide. After drying the synthesis products

overnight at 120 °C, they were stored under ambient conditions and used as such in the interlayer expansion treatment. TG analysis under O_2 (*vide infra*) indicates that under these conditions, both of these materials realize a weight loss of ca. 20 wt.% in the temperature range from room temperature to 800 °C due to the loss of water (less than 2 wt.% weight loss below 120 °C), decomposition and removal of the SDA and condensation of the neighboring silicate layers [10].

2.1.2 Interlayer expansion and incorporation of thiol groups

RUB-36 and RUB-39 were interlayer expanded with (3-mercaptopropyl)methyldimethoxysilane (3-MPS, Fluka 95%) as silylating agent. 200 mg of the layered precursor was added to 12 ml of an aqueous 0.3 M HCl solution. The suspension was stirred for 5 min at room temperature in a Teflon cup. The 3-MPS was slowly added under stirring. 2 mmol 3-MPS was used per g layered precursor. After stirring for another 15 min, the Teflon cup was inserted in a stainless steel autoclave, sealed and treated hydrothermally at 150 °C for 24 h. The suspension was recovered and the solid product was washed repeatedly with water via centrifugation until the pH of the supernatant was neutral. The obtained material was dried overnight at 60 °C. For comparison, the expansions were also performed with DCDMS instead of 3-MPS.

Interlayer expansion of RUB-36 and RUB-39 with DCDMS results in materials referred to as COE-3 and COE-1, respectively [9, 11]. The materials obtained with 3-MPS as silylating agent are correspondingly labeled HS-COE-3 and HS-COE-1. A schematic overview of the different treatments and names for RUB-36 related materials can be found in figure 1.

2.1.3 Oxidation of the thiol groups

For the oxidation of the incorporated thiol groups to the corresponding sulphonic acid groups, an aqueous hydrogen peroxide solution was used as oxidant with methanol or ethanol as solvent. Starting from the procedure optimized by Bossaert *et al.* [23] for the oxidation of thiol groups incorporated in ordered mesoporous silica, a screening – guided by the detection of thiol and propylsulphonic groups in ^{13}C CP MAS NMR - was performed to find the optimal oxidation conditions for the case of HS-COE-3 and HS-COE-1. In a typical oxidation treatment, the powder was treated with 20.4 g H_2O_2 solution (35 – 50 wt.%) per g material for 24 h. A ratio of two parts H_2O_2 solution to three parts solvent was used. The amount of H_2O_2, the H_2O_2 concentration, the solvent, the number of oxidation steps and the treatment temperature were varied. After the H_2O_2 treatment, the powder was washed three times with water and suspended for 4 h in 0.1 M H_2SO_4 (60 ml of acid solution per g of solid).The powder was washed with water until neutral washings were obtained and dried at 60 °C. The oxidized materials were labeled HO_3S-COE-3-x and HO_3S-COE-1-x with x referring to the applied oxidation treatment (table 1).

Table 1. Overview of the applied oxidation conditions.

2.2 Characterization

Powder X-ray diffraction patterns were collected on a STOE Stadi MP diffractometer in Debye-Scherrer geometry with Cu-Kα_1 radiation and equipped with a linear position-sensitive detector (PSD) (6 °2θ window). The samples were measured in a capillary sample holder. The morphology of the crystals was investigated with scanning electron microscopy (SEM) on a Philips XL30 FEG. N_2-physisorption isotherms were recorded on a Micromeritics 3Flex surface analyzer at 77 K . Prior to measurement, the samples were evacuated under vacuum at 393 K for 16 h. The amount of incorporated 3-MPS was determined using thermogravimetric analysis on a TGA Q500 (TA Instruments). Samples were heated at 10 °C/min from room temperature to 800 °C under O_2-flow (O_2:N_2 = 9). The amount of water desorbing below 120 °C was taken into account in determining the amount of incorporated 3-MPS. The acid capacities were determined using titration based on Zeidan *et al.* [26]. 50 mg of catalyst was stirred at room temperature in 15 ml of 2M NaCl for 48 h. The suspension was filtered, rinsed with water and the filtrate was titrated with 0.01 N NaOH using phenol red as indicator. Titrations were repeated three times per catalyst and the average was reported.

^{29}Si MAS NMR spectra were recorded on a 7.0 T Bruker AMX300 spectrometer (^{29}Si resonance frequency 59.6 MHz). 4000 scans were accumulated with a recycle delay of 60 s. The pulse length was 5.0 μs. The samples were packed in 4 mm zirconia rotors and a 5000 Hz spinning frequency was used. ^{13}C CP MAS NMR spectra were recorded on a Bruker Avance400 spectrometer (9.4 T), with a ^{13}C resonance frequency of 100.6 MHz. 22000 scans were accumulated with a recycle delay of 10 s. The contact time was 4.0 ms. The samples were packed in 4 mm zirconia rotors (spinning frequency 6000 Hz). Tetramethylsilane was used as chemical shift reference in both ^{29}Si MAS NMR and ^{13}C CP MAS NMR.

2.3 Catalytic testing

Tetrahydropyranylation reactions of different alcohols were performed in presence of excess 3,4-dihydro-2H-pyran (DHP, molar ratio DHP : alcohol 2). For the tetrahydropyranylation of ethanol, 30 mg of catalyst was weighed into a 10 mL crimp cap vial with a magnetic stirring bar. 1.2 mmol ethanol, 2.4 mmol DHP and 7 mL heptane as solvent were added. The vial was closed, placed into a heated copper block at 70 °C and stirred at 500 rpm. A hot filtration test was performed by removing the catalyst at reaction temperature from the reaction mixture by filtration and transferring the filtrate quickly into a fresh, hot reactor. Tetrahydropyranylation of 2-butanol was performed using 0.6 mmol 2-butanol and 1.2 mmol DHP in 7 mL heptane. Competitive

tetrahydropyranylation reactions of ethanol and cholesterol were performed using 0.3 mmol cholesterol, 0.3 mmol ethanol, 1.2 mmol DHP and 7 mL heptane. The reaction was also performed with Amberlyst-15 as a non-shape selective catalyst containing sulphonic acid groups. The amount of Amberlyst-15 was adjusted to obtain the same molar amount of sulphonic groups as for the other materials. Samples (0.1 ml) were taken periodically and analyzed on a Shimadzu 2014 GC equipped with an FID and 60m CP Sil8 column. Peaks were identified by injecting authentic samples and by GC-MS.

3 Results and discussion

3.1 Incorporation of (3-mercaptopropyl)methyldimethoxysilane

Powder X-ray diffraction patterns for HS-COE-3 and HS-COE-1 are shown in figures 2 and 3. For both materials, the shift of the first and most intense diffraction line towards lower 2θ values indicates an increase in the interlayer distance compared to the layered precursor and the corresponding product of topotactic condensation. For comparison, *d*-spacings and reflection angles are shown in table 2. The interlayer distances for the materials expanded with 3-MPS are very similar to the values obtained for DCDMS expanded materials. The ^{29}Si MAS NMR spectrum of HS-COE-3 (figure 4) shows the presence of Q^4 (-112 ppm, -116 ppm) and some residual Q^3 (-104 ppm) species [9]. At -14 ppm, the Si signal of the bridging group derived from 3-MPS can be observed. Also for HS-COE-1 (figure 5), the Si bridging atom (at -13 ppm) is clearly present in addition to the layer related Q^4 (-108 ppm, -114 ppm) and Q^3 (-102 ppm) species. The Q^3/Q^4 ratios for HS-COE-1 and HS-COE-3, obtained by integrating the corresponding areas, are 0.09 and 0.02, respectively. They clearly show a significant reduction in the relative amount of Q^3 species compared to the layered precursors, as for both types of layered precursors, the theoretical and experimentally observed Q^3/Q^4 ratio amounts to 0.29 [27]. This indicates that Q^3 species have been consumed in the linking reaction of 3-MPS with the layers. The amount of incorporated 3-MPS was estimated from both the ^{29}Si MAS NMR and TG analysis of the expanded materials (table 3). Full occupation of all possible linker sites in COE-3 and COE-1 would result in a unit cell composition of $[Si_{20}O_{38}(CH_3)_2(CH_2CH_2CH_2SH)_2]$ with a ratio of layer-related Si to linker Si of 9 to 1 (1 : 0.11) for both types of layers [9]. Integration of the 3-MPS related signal and the layer related signals results in a ratio of 1 : 0.12 and 1 : 0.09 for HS-COE-3 and HS-COE-1, respectively. These values are in close agreement with the maximum incorporation of 3-MPS. It should be noted that the presence of a significant amount of Q^3 species, especially in the case of HS-COE-1, indicates that not all linking sites are occupied. Part of the 3-MPS may have condensed with another 3-MPS molecule and/or may be present at the outer surface of the crystals. This could explain the weak signal at -20 ppm in the

^{29}Si MAS NMR spectra of both HS-COE-3 and HS-COE-1 [28]. The expected weight loss upon calcination in air for HS-COE-3 and HS-COE-1 is 8.3 wt.% if all linker sites are occupied by 3-MPS. TG analysis shows a slightly higher weight loss for both materials (table 3). This can be ascribed to the loss of residual SDA, the presence of which is also confirmed in ^{13}C CP MAS NMR (figures 6, 7).

Figure 2. Powder XRD patterns of RUB-36 (a), RUB-37 (b), HS-COE-3 (c) and HO_3S-COE-3-E (d).

Figure 3. Powder XRD patterns of RUB-39 (a), RUB-41 (b), HS-COE-1 (c) and HO_3S-COE-1-E (d).

Table 2. Overview of the *d*-spacings corresponding to the first and most intense reflection in the XRD patterns of the layered materials.

Figure 4. ^{29}Si MAS NMR spectrum of HS-COE-3.

Figure 5. ^{29}Si MAS NMR spectrum of HS-COE-1.

Table 3. Physicochemical properties of the thiol and sulphonic acid functionalized materials.

3.2 Oxidation of the incorporated thiol groups

Several oxidation procedures were screened to find the optimal oxidation conditions regarding conversion of the thiol groups and number of oxidation steps. Table 1 lists the applied oxidation conditions. The degree of oxidation was monitored using ^{13}C CP MAS NMR (figure 6 and 7). The peak assignments are listed in Table 4. Remarkably, even if the silylating treatment was conducted in drastic conditions (150°C), without any precautions to exclude air, the thiol groups were the major sulfur species observed and only trace amounts of disulfide bridges from oxidation were detected. Although the ^{13}C CP MAS NMR measurement is not fully quantitative, the oxidation of the incorporated thiol groups to sulphonic acid groups can be observed from the disappearance of the peak at 27 ppm and the appearance of a (broad) signal at 54 ppm. Under the conditions used by Bossaert *et al*. [23] for the oxidation of incorporated thiol groups in ordered mesoporous silica, hardly any oxidation occurred, indicating that the thiol groups must be in a less accessible environment. Figure 6 clearly shows that increasing the oxidation temperature and the H_2O_2 concentration results in an increased conversion of the thiol groups. Increasing the number of oxidation steps results in a higher number of sulphonic acid groups as well (figure 6 c,d). For HO_3S-COE-3-E the signal corresponding to the thiol groups is no longer detected. Also for HO_3S-COE-1-E the thiol oxidation is essentially complete (figure 7).

Table 4. Chemical shift of different C-atoms in the interlayer expanded and oxidized materials in ^{13}C CP MAS NMR (peak assignment based on ref. [29]).

Figure 6. ^{13}C CP MAS NMR of HS-COE-3 (a), HO_3S-COE-3-A (b), HO_3S-COE-3-B (c), HO_3S-COE-3-C (d), HO_3S-COE-3-D (e), HO_3S-COE-3-E (f) and HO_3S-COE-3-F (g). Weak signals at 58, 52 and 8 ppm in (a) are attributed to residual SDA [3, 30].

Figure 7. ^{13}C CP MAS NMR of HS-COE-1 (a), HO_3S-COE-1-B (b) and HO_3S-COE-1-E (c). Weak signals at 67, 51 and 9 ppm in (a) are attributed to residual SDA [11].

After the more harsh oxidation treatments, the XRD-patterns (figure 2, 3), especially of HO_3S-COE-1-E, show some peak broadening indicating a partial loss of crystallinity. This is in agreement with the SEM images (figure 8f) that show the formation of some debris after oxidation treatment, though the plate-like morphology is generally very well preserved. BET surface areas before and after oxidation treatment E (table 3) show very low N_2 uptakes. These can be explained by the limited micropore area available due to the additional mass of the mercaptopropyl and propylsulphonic groups. The limited accessibility of the pores to N_2 in physisorption experiments, however, does not exclude the access of reactants in liquid phase processes, as will be demonstrated by the catalytic properties.

Figure 8. SEM images of RUB-36 (a), HS-COE-3 (b), HO_3S-COE-3-E (c), RUB-39 (d), HS-COE-1 (e) and HO_3S-COE-1-E (f) (scale bar = 10 µm).

In the TG analysis of the materials after the oxidation treatment (table 3), an increased weight loss is expected because of the higher molecular weight of the propylsulphonic group compared to the mercaptopropyl group. However, for HO_3S-COE-3-E, this increase is very small. The rather harsh oxidation conditions may have hydrolyzed part of the linkers resulting in a lower weight loss. Furthermore some residual SDA is removed during the several steps of the oxidation treatment, as the SDA is no longer detected in the ^{13}C CP MAS NMR. On the other hand, the increase in weight loss after oxidation is more clear in the case of HO_3S-COE-1-E.

3.3 Catalytic properties

Tetrahydropyranylation reactions can be catalyzed by a number of different catalysts, like zeolites [31-33] , aluminum phosphates [34], sulfonated charcoal [35], polystyrene supported Lewis acids [36], etc. An alternative method is using sulfonic acid functionalized materials such as sulfonic acid functionalized MCM-41 [20]. The HO_3S-COE-1 and HO_3S-COE-3 type materials

are analogous to the latter type of materials but their active sites are located in a spatially more restricted environment.

Tetrahydropyranylation reactions of ethanol and 2-butanol show the presence of accessible acid sites in both HO_3S-COE-3-E and HO_3S-COE-1-E (figures 9 and 10). On mass basis, HO_3S-COE-3-E shows a higher activity in both reactions, even though it has a lower acid site loading (table 3). However, the TOF numbers of HO_3S-COE-3-E are higher for both ethanol and 2-butanol (table 5). The hot filtration tests in the ethanol tetrahydropyranylation show no increase in conversion after catalyst removal, indicating that the reaction is fully heterogeneous.

Figure 9. Ethanol conversion in the tetrahydropyranylation with HO_3S-COE-3-E (a) and HO_3S-COE-1-E (b). Dashed lines show the hot filtration test.

Figure 10. 2-butanol conversion in the tetrahydropyranylation with HO_3S-COE-3-E (x) and HO_3S-COE-1-E (+).

Table 5. TOF in the tetrahydropyranylation of ethanol and 2-butanol.

To demonstrate the shape-selective properties of the interlayer expanded materials with functionalized linker groups, competitive tetrahydropyranylation reactions were performed. Ethanol and cholesterol were used as small resp. bulky alcohols. Although their reactivity is not the same, differences in relative reaction rates can be used to demonstrate shape selectivity. Figure 11 shows the alcohol conversion as a function of time for different catalysts. Even with the macroporous Amberlyst resin, ethanol is converted more rapidly than cholesterol. However, the bulky cholesterol is converted significantly more slowly than ethanol on the interlayer expanded zeolites. This clearly shows that the active sites are located in a restricted environment in between the layers. As cholesterol is too large to fit into the pores of the zeolite materials, its conversion should be attributed to the presence of sulphonic acid sites at the outer surface of the crystals or at the pore entrance.

Figure 11. Conversion of ethanol (x) and cholesterol (+) in the competitive tetrahydropyranylation with HO_3S-COE-3-E (a), HO_3S-COE-1-E (b) and Amberlyst-15 (c).

4 Conclusions

The layered zeolite precursors RUB-36 and RUB-39 were successfully interlayer expanded using 3-MPS as silylating agent. Complete oxidation of the incorporated thiol groups to sulphonic acid groups was obtained, while preserving the layer structure. The competitive tetrahydropyranylation of ethanol and cholesterol showed that both materials possess shape-

selective properties owing to the introduction of the catalytically active sites in between the layers, with a relatively faster conversion of small aliphatic alcohols than of large, sterically hindered alcohols.

Acknowledgements

T.D.B. acknowledges F.W.O. – Vlaanderen (Research Foundation – Flanders) for a doctoral fellowship. Support of BASF SE under the INCOE framework is acknowledged. The authors thank dr. K. Houthoofd for collecting the NMR spectra.

References

[1] C. T. Kresge, W. J. Roth, K. G. Simmons, J. C. Vartuli, US Patent 5 229 341 (1993), to Mobil Oil Corp.

[2] W. J. Roth, C. T. Kresge, J. C. Vartuli, M. E. Leonowicz, A. S. Fung, S. B. McCullen, Stud. Surf. Sci. Catal. 94 (1995) 301-308.

[3] Z. Zhao, W. Zhang, P. Ren, X. Han, U. Müller, B. Yilmaz, M. Feyen, H. Gies, F.-S. Xiao, D. De Vos, T. Tatsumi, X. Bao, Chem. Mater. 25 (2013) 840-847.

[4] P. Wu, J. Ruan, L. Wang, L. Wu, Y. Wang, Y. Liu, W. Fan, M. He, O. Terasaki, T. Tatsumi, J. Am. Chem. Soc. 130 (2008) 8178-8187.

[5] A. Corma, V. Fornes, S. Pergher, T. L. Maesen, J. Buglass, Nature 396 (1998) 353-356.

[6] T. Ikeda, S. Kayamori, Y. Oumi, F. Mizukami, J. Phys. Chem. C 114 (2010) 3466-3476.

[7] S. Maheshwari, E. Jordan, S. Kumar, F. S. Bates, R. L. Penn, D. F. Shantz, M. Tsapatsis, J. Am. Chem. Soc. 130 (2008) 1507-1516.

[8] S. Inagaki, T. Yokoi, Y. Kubota, T. Tatsumi, Chem. Commun. (2007) 5188-5190.

[9] H. Gies, U. Müller, B. Yilmaz, M. Feyen, T. Tatsumi, H. Imai, H. Zhang, B. Xie, F. S. Xiao, X. Bao, Chem. Mater. 24 (2012) 1536-1545.

[10] Y. Wang, H. Gies, B. Marler, U. Müller, Chem. Mater. 17 (2005) 43-49.

[11] H. Gies, U. Müller, B. Yilmaz, T. Tatsumi, B. Xie, F. S. Xiao, X. Bao, W. Zhang, D. D. Vos, Chem. Mater. 23 (2011) 2545-2554.

[12] F.-S. Xiao, B. Xie, H. Zhang, L. Wang, X. Meng, W. Zhang, X. Bao, B. Yilmaz, U. Müller, H. Gies, H. Imai, T. Tatsumi, D. De Vos, ChemCatChem 3 (2011) 1442-1446.

[13] B. Tijsebaert, M. Henry, H. Gies, F. S. Xiao, W. P. Zhang, X. H. Bao, H. Imai, T. Tatsumi, U. Müller, B. Yilmaz, P. Jacobs, D. De Vos, J. Catal. 282 (2011) 47-53.

[14] A. Corma, U. Diaz, M. E. Domine, V. Fornés, J. Am. Chem. Soc. 122 (2000) 2804-2809.

[15] B. Yilmaz, U. Muller, M. Feyen, H. Zhang, F.-S. Xiao, T. De Baerdemaeker, B. Tijsebaert, P. Jacobs, D. De Vos, W. Zhang, X. Bao, H. Imai, T. Tatsumi, H. Gies, Chem. Commun. 48 (2012) 11549-11551.

[16] A. Corma, U. Díaz, V. Fornés, J. L. Jordá, M. Domine, F. Rey, Chem. Commun. (1999) 779-780.

[17] I. Domínguez, V. Fornés, M. J. Sabater, J. Catal. 228 (2004) 92-99.

[18] V. Ayala, A. Corma, M. Iglesias, J. Rincon, F. Sanchez, J. Catal. 224 (2004) 170-177.

[19] A. Corma, U. Díaz, T. García, G. Sastre, A. Velty, J. Am. Chem. Soc. 132 (2010) 15011-15021.

[20] M. H. Lim, C.F. Blanford, A. Stein, Chem. Mater. 10 (1998) 467-470.

[21] Y. Ide, N. Kagawa, M. Itakura, I. Imae, M. Sadakane, T. Sano, ACS Appl. Mater. Interfaces 4 (2012) 2186-2191.

[22] W.M. Van Rhijn, D.E. De Vos, B.F. Sels, W.D. Bossaert, P.A. Jacobs, Chem. Commun. (1998) 317-318.

[23] W. D. Bossaert, D. E. De Vos, W. M. Van Rhijn, J. Bullen, P. J. Grobet, P. A. Jacobs, J. Catal. 182 (1999) 156-164.

[24] S. Shylesh, S. Sharma, S. P. Mirajkar, A. P. Singh, J. Mol. Cat. A 212 (2004) 219-228.

[25] E. Cano-Serrano, G. Blanco-Brieva, J. M. Campos-Martin, J. L. G. Fierro, Langmuir 19 (2003) 7621-7627.

[26] R. K. Zeidan, V. Dufaud, M. E. Davis, J. Catal., 239 (2006) 299-306.

[27] B. Marler, H. Gies, Eur. J. Mineral. 24 (2012) 405-428.

[28] B. A. Ashu-Arrah, J. D. Glennon, K. Albert, J. Chromatogr. A 1222 (2012) 38-45.

[29] W. M. Van Rhijn, Derivatization of renewable organic chemicals with ordered hybrid sulfonic acids, PhD thesis at KU Leuven, 2001, pp. 179.

[30] T. Ikeda, S. Kayamori, F. Mizukami, J. Mater. Chem. 19 (2009) 5518-5525.

[31] I. Rodriguez, M. Climent, S. Iborra, V. Fornes, A. Corma, J. Catal. 192 (2000) 441-447.

[32] N. Narender, K. Suresh Kumar Reddy, M. Arun Kumar, C. N. Rohitha, S. J. Kulkarni, Catal. Lett. 134 (2010) 175-178.

[33] R. Ballini, F. Bigi, S. Carloni, R. Maggi, G. Sartori, Tetrahedron Lett. 38 (1997) 4169-4172.

[34] J. M. Campelo, A. Garcia, F. Lafont, D. Luna, J. M. Marinas, Synth. Commun. 22 (1992) 2335-2342.

[35] H. K. Patney, Synth. Commun. 21 (1991) 2329-2333.

[36] Y. Zhang, Q. Dou, Y. Liu, L. Dai, X. Wang, Y. Chen, Chin. J. Chem. 30 (2012) 2567-2572.

List of figures

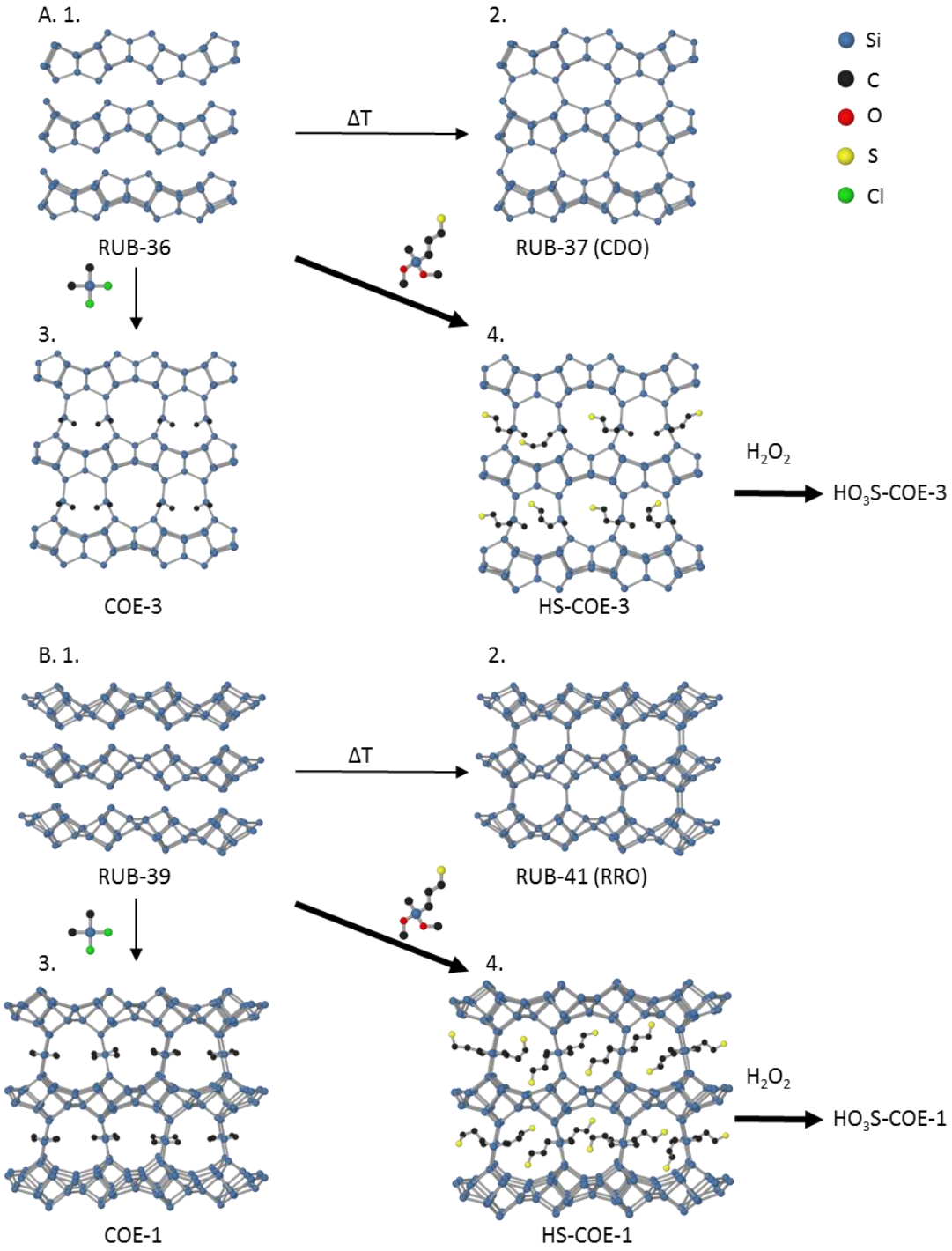

Figure 1. Materials derived from layered zeolite precursors RUB-36 (A) and RUB-39 (B). Displayed are the layered precursors (1) and the products of topotactic condensation (2) and interlayer expansion with DCDMS (3) or with 3-MPS (4) followed by oxidation with H_2O_2. Framework O-atoms and the organic SDAs in the layered precursors are omitted for clarity. In the case of RUB-39, two linking sites eclipsing each other are shown.

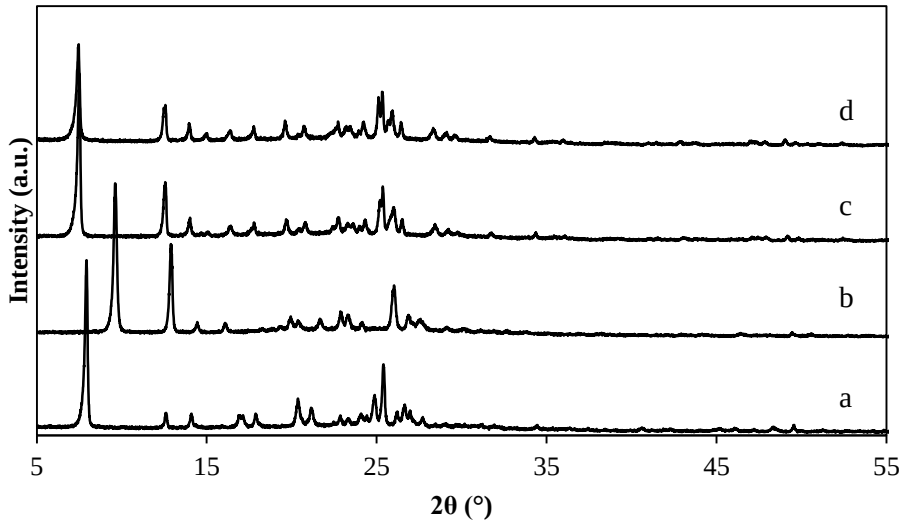

Figure 2. Powder XRD patterns of RUB-36 (a), RUB-37 (b), HS-COE-3 (c) and HO_3S-COE-3-E (d).

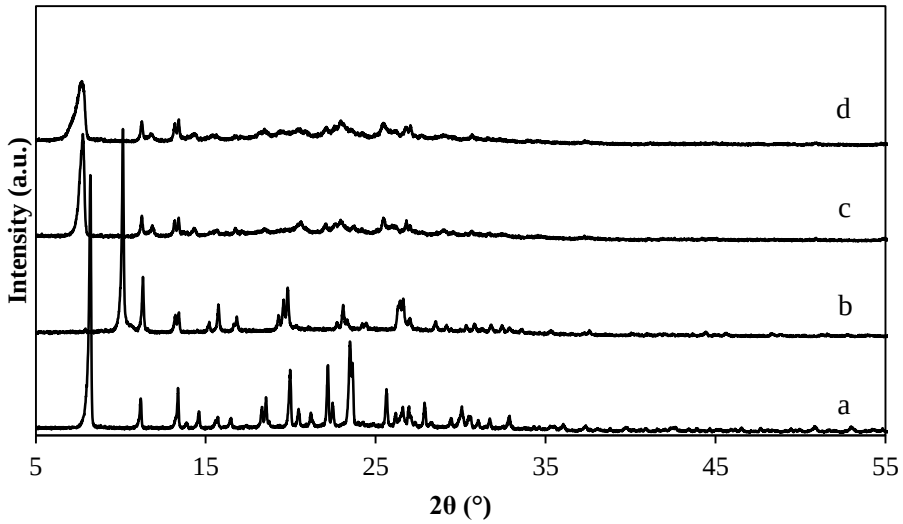

Figure 3. Powder XRD patterns of RUB-39 (a), RUB-41 (b), HS-COE-1 (c) and HO_3S-COE-1-E (d).

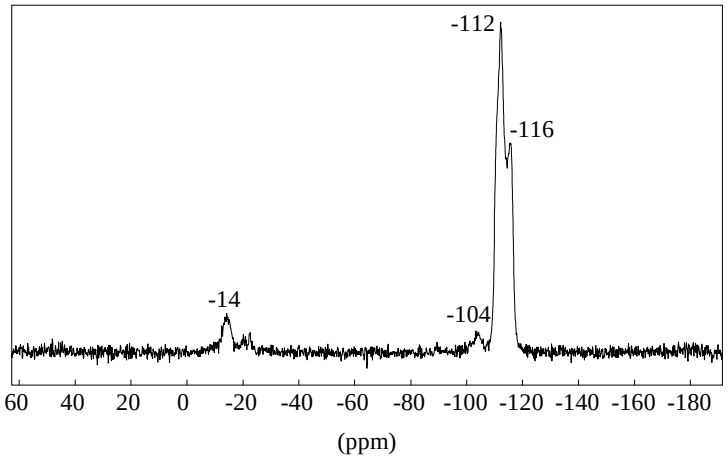

Figure 4. ^{29}Si MAS NMR spectrum of HS-COE-3.

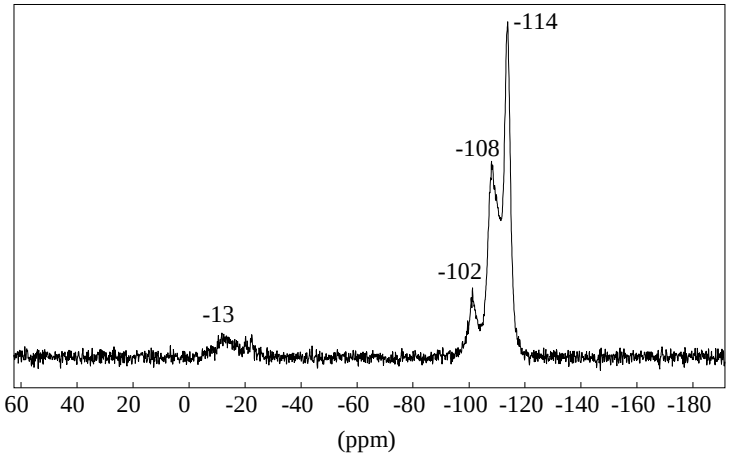

Figure 5. ^{29}Si MAS NMR spectrum of HS-COE-1.

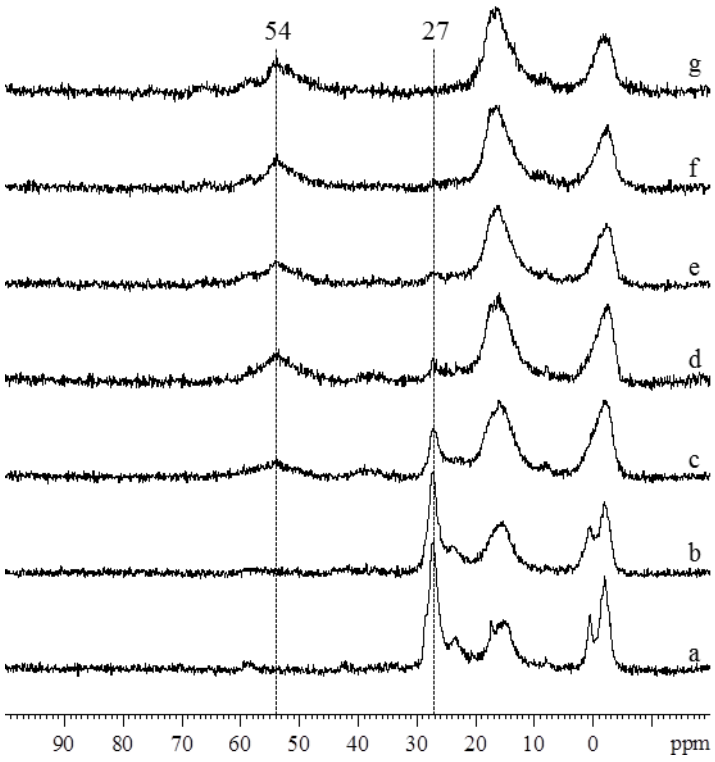

Figure 6. ^{13}C CP MAS NMR of HS-COE-3 (a), HO_3S-COE-3-A (b), HO_3S-COE-3-B (c), HO_3S-COE-3-C (d), HO_3S-COE-3-D (e), HO_3S-COE-3-E (f) and HO_3S-COE-3-F (g). Weak signals at 58, 52 and 8 ppm in (a) are attributed to residual SDA [3, 30].

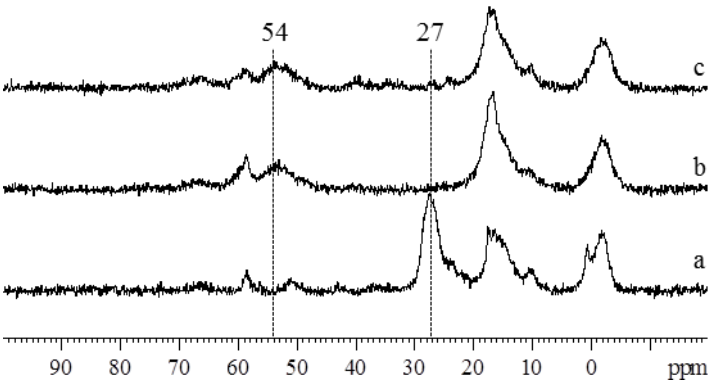

Figure 7. ^{13}C CP MAS NMR of HS-COE-1 (a), HO_3S-COE-1-B (b) and HO_3S-COE-1-E (c). Weak signals at 67, 51 and 9 ppm in (a) are attributed to residual SDA [11].

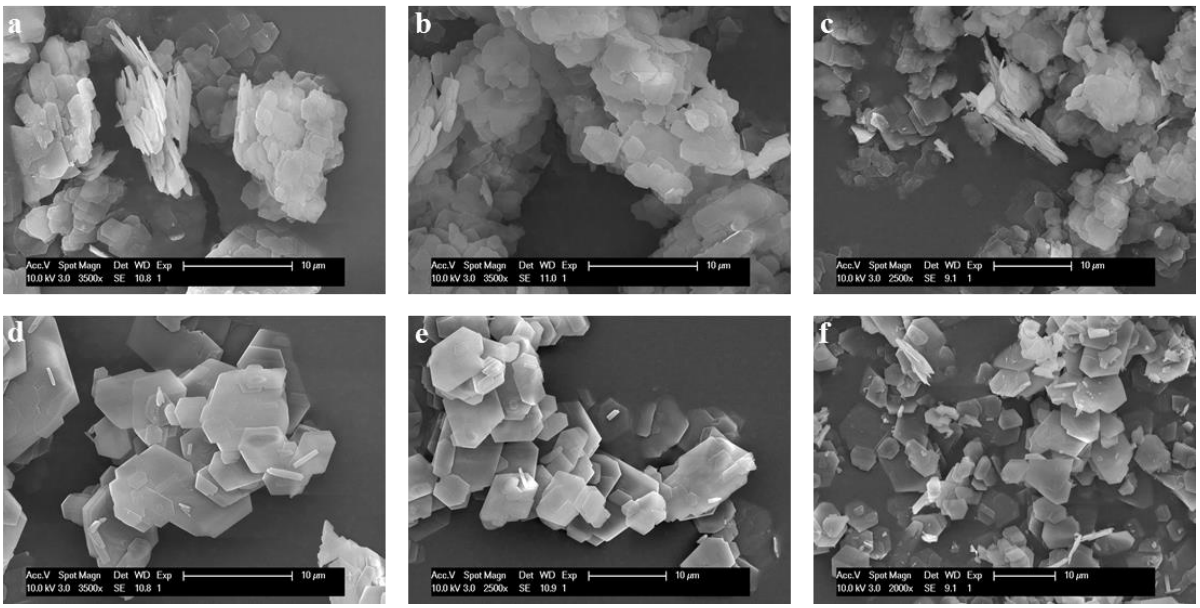

Figure 8. SEM images of RUB-36 (a), HS-COE-3 (b), HO_3S-COE-3-E (c), RUB-39 (d), HS-COE-1 (e) and HO_3S-COE-1-E (f) (scale bar = 10 µm).

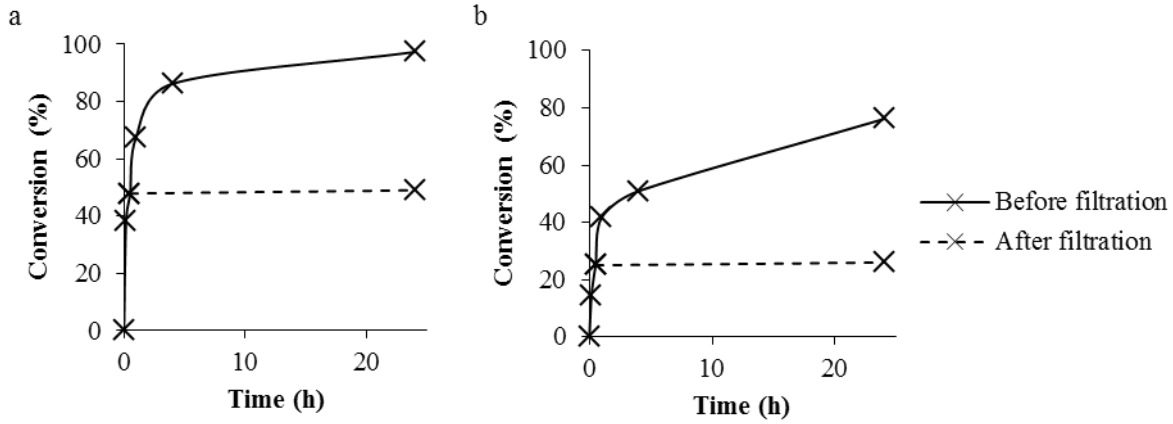

Figure 9. Ethanol conversion in the tetrahydropyranylation with HO_3S-COE-3-E (a) and HO_3S-COE-1-E (b). Dashed lines show the hot filtration test.

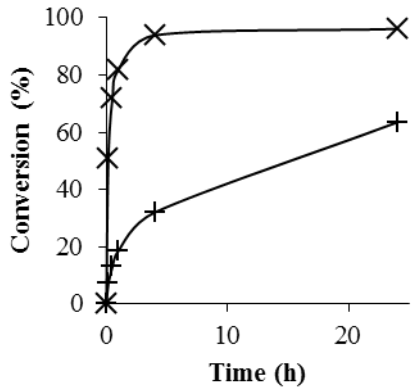

Figure 10. 2-butanol conversion in the tetrahydropyranylation with HO_3S-COE-3-E (x) and HO_3S-COE-1-E (+).

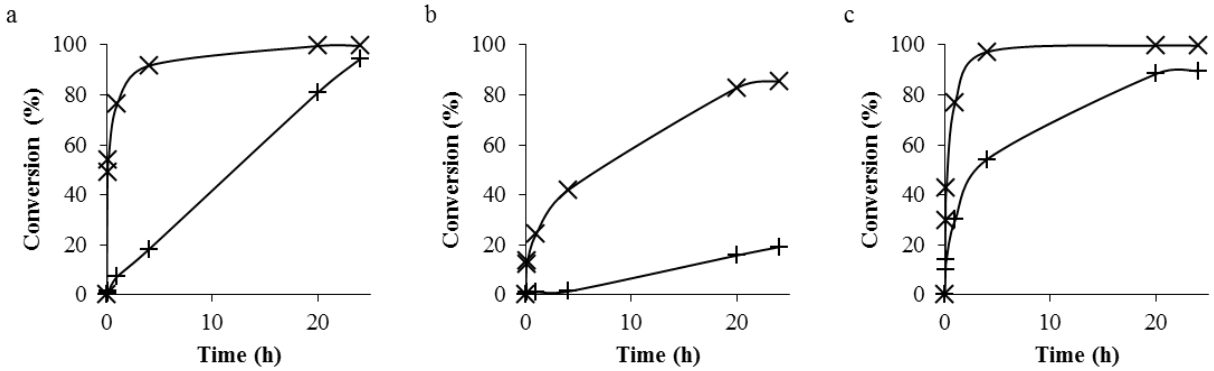

Figure 11. Conversion of ethanol (x) and cholesterol (+) in the competitive tetrahydropyranylation with HO_3S-COE-3-E (a), HO_3S-COE-1-E (b) and Amberlyst-15 (c).

List of tables

Table 1. Overview of the applied oxidation conditions.

Treatment	H_2O_2 amount [a]/ conc. [b]	T (°C)	Solvent	Number of oxidation steps
A [c]	2.04 / 35	r.t. [d]	Methanol	1
B	20.4 / 35	50	Methanol	1
C	20.4 / 35	50	Methanol	4
D	20.4 / 35	70	Ethanol	1
E	20.4 / 50	70	Ethanol	1
F	20.4 / 50	70	Ethanol	4

[a] g H_2O_2 solution per g material. [b] wt. %. [c] Optimized conditions of Bossaert *et al.* [23]. In this case, a ratio of one part H_2O_2 solution to three parts of methanol was used. [d] Room temperature.

Table 2. Overview of the *d*-spacings corresponding to the first and most intense reflection in the XRD patterns of the layered materials.

Material	2θ (°)	*d*-spacing (Å)
RUB-36	7.9	11.1
RUB-37	9.6	9.2
COE-3	7.5	11.7
HS-COE-3	7.5	11.8
RUB-39	8.2	10.8
RUB-41	10.1	8.7
COE-1	7.9	11.2
HS-COE-1	7.8	11.4

Table 3. Physicochemical properties of the thiol and sulphonic acid functionalized materials.

	Organic content (wt.% loss) [a]	**SO_3H (mmol/g)** [b]	**BET area (m^2/g)**	**V_{micro} (cm^3/g)** [c]
HS-COE-3	14.3	-	10.2	<0.001
HS-COE-1	12.0	-	4.4	<0.001
HO_3S-COE-3-E	14.8	0.31	26.5	0.002
HO_3S-COE-1-E	13.7	0.50	24.8	0.004

[a] wt.% lost in the range 120-550 °C after taking into account the desorption of water below 120 °C. [b] Determined via titration. [c] From t-plot analysis of the N_2 physisorption isotherms.

Table 4. Chemical shift of different C-atoms in the interlayer expanded and oxidized materials in ^{13}C CP MAS NMR (peak assignment based on ref. [29]).

C-atom	**Chemical shift (ppm)**
Si-**C**H_3	0
Si-**C**$H_2CH_2CH_2SH$	13
Si-CH_2**C**H_2CH_2SH	27
Si-CH_2CH_2**C**H_2SH	27
Si-CH_2**C**H_2CH_2S-SCH_2**C**H_2CH_2-Si	23
Si-CH_2CH_2**C**H_2S-S**C**$H_2CH_2CH_2$-S	41
Si-**C**$H_2CH_2CH_2SO_3H$	11
Si-CH_2**C**$H_2CH_2SO_3H$	18
Si-CH_2CH_2**C**H_2SO_3H	54

Table 5. TOF in the tetrahydropyranylation of ethanol and 2-butanol.

	TOF (h^{-1}) [a] ethanol	**TOF (h^{-1}) [a] 2-butanol**
HO_3S-COE-3-E	87	52
HO_3S-COE-1-E	34	8

[a] mol alcohol converted per mol acid sites per h, based on the acid site density determined via titration.